Magnesium-Induced Assembly of a Complete DNA Polymerase Catalytic Complex

ARTICLE *in* STRUCTURE · MAY 2006

Impact Factor: 5.62 · DOI: 10.1016/j.str.2006.01.011 · Source: PubMed

Published in final edited form as:
Structure. 2006 April ; 14(4): 757–766.

Magnesium Induced Assembly of a Complete DNA Polymerase Catalytic Complex

Vinod K. Batra[*], **William A. Beard**[*], **David D. Shock**, **Joseph M. Krahn**, **Lars C. Pedersen**, and **Samuel H. Wilson**[†]

Laboratory of Structural Biology, National Institute of Environmental Health Sciences, National Institutes of Health, P.O. Box 12233, Research Triangle Park, North Carolina 27709

Summary

The molecular details of the nucleotidyl transferase reaction have remained speculative, as strategies to trap catalytic intermediates for structure determination utilize substrates lacking the primer terminus 3'–OH and catalytic Mg^{2+} resulting in an incomplete and distorted active site geometry. Since the geometric arrangement of these essential atoms will impact chemistry, structural insight into fidelity strategies has been hampered. Here we present the first crystal structure of a pre-catalytic complex of a DNA polymerase with bound substrates that include the primer 3'–OH and catalytic Mg^{2+}. This catalytic intermediate was trapped with a non-hydrolyzable deoxynucleotide analogue. Comparison with two new structures of DNA polymerase β lacking the 3'–OH or catalytic Mg^{2+} is described. These structures provide direct evidence that both atoms are required to achieve a proper geometry necessary for an in-line nucleophilic attack of O3' on the αP of the incoming nucleotide.

Introduction

DNA polymerases must select and incorporate a complementary deoxynucleotide from a pool of structurally similar molecules to preserve the integrity of the genome. Failure to preserve Watson-Crick base pairing rules usually results in deleterious biological consequences. Although the fidelities of DNA polymerases vary widely, the catalytic efficiencies by which they insert incorrect nucleotides is only weakly dependent on the identity of the polymerase. These differences in fidelities are due to the divergent abilities of polymerases to insert the right nucleotide (Beard et al., 2002); low fidelity enzymes insert the correct nucleotide slowly, whereas high fidelity DNA polymerases insert the correct nucleotide rapidly (Beard and Wilson, 2003).

The structural characterization of DNA polymerases from different families indicates that these enzymes have a modular domain and subdomain organization (Beard and Wilson, 2003, Steitz, 1999). The polymerase domain is generally composed of 3 subdomains with distinct functional roles. The catalytic subdomain, also referred to as the C–subdomain or palm, contributes two-structurally conserved aspartate residues that coordinate Mg^{2+}. Based on the mechanism for the 3'–5' exonuclease of Klenow fragment, a 'two-metal ion' mechanism for nucleotidyl transfer has been proposed (Beese and Steitz, 1991, Steitz et al., 1994). The catalytic metal (metal A) is thought to lower the pK_a of the 3'-OH of the growing primer terminus while the nucleotide binding metal (metal B) coordinates the triphosphate moiety hastening binding of

†Correspondence: wilson5@niehs.nih.gov.
*These authors contributed equally to this work.

Accession Numbers

Coordinates and structure factors for the ddCTP, dUMPNPP (Na^+/Mg^{2+}) and dUMPNPP (Mg^{2+}/Mg^{2+}) complexes have been deposited in the RSCB Protein Data Bank with accession codes 2FMP, 2FMQ, and 2FMS, respectively.

the incoming nucleotide. Additionally, metal B assists PP_i dissociation. Both metals are believed to stabilize the proposed penta-coordinated transition state of the nucleotidyl transferase reaction.

DNA polymerase (pol) β belongs to the X-family of DNA polymerases and is a repair enzyme that has a key role in the base excision repair of simple DNA lesions (Beard and Wilson, 2000). Due to its small size (39 kDa), lack of a proofreading exonuclease, and many structural, kinetic, and mechanistic features it shares with other DNA polymerases, it is an ideal model system for structural studies. Although pol β exhibits unique structural attributes that reflect its cellular role, the arrangement of active site residues and substrates are remarkably similar to other DNA polymerases (Steitz et al., 1994, Steitz, 1999). Structures of pol β exist for the apoenzyme (Sawaya et al., 1994) and with non-gapped DNA (Pelletier et al., 1994), gapped DNA (Sawaya et al., 1997), lesion-containing DNA (Krahn et al., 2003, Prasad et al., 2005), mismatched DNA in the active site (Krahn et al., 2004), and mismatched DNA at the primer terminus (Batra et al., 2005). These various structures provide a context to interpret structural differences imposed by alternate ligands.

The structures of ternary substrate complexes (pol/DNA/dNTP) have been solved for members of several polymerase families providing valuable insights into substrate selection and chemistry (Table 1). However, these catalytic intermediates were trapped for structure determination by using a dideoxy-terminated primer (lacks O3') or by using a divalent metal, such as Ca^{2+}, that does not support insertion. In each case, the active site geometry for the catalytic metal is distorted owing in part to the longer coordination distances induced with a larger metal such as Ca^{2+}, or the removal of the catalytic nucleophile (O3'), an atom postulated to provide an important ligand for the catalytic metal (Steitz et al., 1993). The distorted geometries of these pre-catalytic complexes have hindered detailed analyses of active site geometries as it pertains to the influence of aberrant DNA (lesions and mismatches) or nucleotide (right versus wrong) substrates on catalytic function. Furthermore, the lack of reference structures exhibiting good active site geometry for DNA polymerases from different polymerase families precludes detailed conclusions regarding structure and chemistry as it relates to function.

By using a non-hydrolysable dUTP analogue, we have determined the structure of a pre-catalytic complex of pol β that includes the catalytic Mg^{2+} and O3' of the primer terminus. For the first time, there is direct evidence that the catalytic Mg^{2+} coordinates the primer O3', induces subtle conformational rearrangements resulting in good octahedral geometry, and positions O3' for an in-line nucleophilic attach on αP of the incoming nucleotide. By employing a similar approach with alternate substrates or DNA polymerases, similarities and/or differences in active site geometries can be reliably assessed.

Results and Discussion

High Resolution Ternary Substrate Complex with Dideoxy-terminated Primer

Using the strategy of employing a dideoxy-terminated primer to trap a ternary substrate complex, previously reported structures of pol β failed to reveal the complete inner coordination sphere of the catalytic metal (Pelletier et al., 1994, Sawaya et al., 1997). We have collected new data and determined a high-resolution (1.65 Å) structure of pol β (Table 2). The new structure provides important details related to the coordination and identity of the ion bound in the catalytic metal site. A water molecule that had been suggested to participate in the octahedral coordination sphere of the catalytic magnesium can now be observed (S2 in Figure 1A). The sixth coordinating ligand is proposed to be O3' of the primer terminus that is missing in this structure (see below). Additionally, the sugar pucker of the dideoxy-terminated primer is C3'-endo, similar to that observed in the well-defined structure of the ternary complex of

Bacillus DNA polymerase I fragment (Johnson et al., 2003), an A-family member, and a conformation commonly observed in A-form DNA.

Most importantly, however, the ion occupying the catalytic metal site in this high-resolution structure appears to be Na^+ rather than Mg^{2+}. Since Mg^{2+} has a low electron density and has the same number of electrons as Na^+ and water, it is difficult to unambiguously assign magnesium ions in protein crystal structures. The identity of this ion is based on the average coordination distance of the coordinating ligands (2.38 Å; Figure 2 and Table 3). This distance is similar to that expected of Na^+ (2.42 Å) (Harding, 2002) rather than Mg^{2+} (2.07 Å) (Harding, 2001), observed in accurately determined small molecule structures (Cambridge Structural Database). Indeed, the average coordination distance observed for the six inner sphere oxygen ligands of the ion in the nucleotide metal B site is consistent with Mg^{2+} occupying this site (2.08 Å, Figures 1B and 2). The penta-coordination geometry of the cation occupying the catalytic metal site is distorted, presumably due to the lack of one of the coordinating ligands (primer terminus O3'). Further, employing the bond-valence method is consistent with the ion occupying the catalytic metal site as Na^+ rather than Mg^{2+} (Müller et al., 2003). The average coordination distance observed in our previously reported ternary complex structure of pol β is also consistent with Na^+ occupying the catalytic metal site, Figure 2 (Sawaya et al., 1997).

Ternary Substrate Complex with Primer 3'-OH

The catalytic metal sites of most previously determined substrate pre-catalytic complex structures of DNA polymerases are missing a critical coordinating ligand, O3' of the primer terminus (Table 1). Since 3'-O^- serves as the attacking nucleophile, the position and coordination geometry is expected to have important ramifications for transition state development. Accordingly, we have determined a structure of a ternary complex that includes 3'–OH of the primer terminus. This was achieved by using a commercially available dNTP analogue, 2'-deoxy-uridine-5'-(α,β)-imido triphosphate (dUMPNPP). The bridging oxygen between the α- and β-phosphates is replaced with nitrogen in this dUTP analogue which prevents insertion. DNA polymerases efficiently insert dUTP since it closely resembles dTTP and it does not alter Watson-Crick hydrogen bonding. DNA polymerase β inserts dUTP with the same efficiency as dTTP (Figure 3A) and is competitively inhibited by dUMPNPP (K_i = 0.9 μM; Figure 3B).

A crystal of the binary single-nucleotide gapped DNA complex was grown and the nucleotide analogue soaked into the crystal (Batra et al., 2005). This crystal diffracted at 2.2 Å, and clear density for the O3' on the primer terminus was observed (Figure 4A). In addition, replacing the bridging oxygen between the α- and β-phosphates with nitrogen did not significantly distort the triphosphate moiety of the incoming nucleotide as evidenced by the equivalent position of the phosphates for ddCTP and dUMPNPP (Figure 4B). Unexpectedly however, the primer terminal O3' was 4.7 Å from the αP of the incoming dUMPNPP and 3.5 Å from the ion in catalytic metal site (Figure 4C). Despite the presence of magnesium in the crystallization solution, the ion in the catalytic metal site was consistent with Na^+ rather than Mg^{2+} (Figure 2). Here, as in the high-resolution structure described above, the identity of the nucleotide binding metal B was consistent with Mg^{2+} displaying good octahedral geometry and an average coordination distance of 2.07 Å (Figures 2 and 4B).

Pre-catalytic Complex with Mg^{2+} Occupying the Catalytic Metal Site

The nucleotide analogue had been soaked into the binary complex crystals in the presence of 180 mM sodium acetate and 10 mM $MgCl_2$. To provide Mg^{2+} a better opportunity to bind to the catalytic metal site, the Mg^{2+}/Na^+ ratio was increased from 0.06 to 2.22 (see Experimental Procedures). The resulting crystal diffracted at 2.0 Å and there is clear density for O3' of the primer terminus (Figure 5). The octahedral coordination geometry (Figure 6A) and average

coordination distance for the oxygen ligands with the ion in site A was consistent with Mg^{2+} occupying this site (Figures 2). Significantly, O3' of the primer terminus is now 2.2 Å from metal A in contrast to the 3.5 Å observed when Na^{+} occupies this site (Figure 7). This repositioning of O3' could occur through a change in the preferred sugar-pucker of the primer terminus. The sugar-pucker of the primer terminus with Mg^{2+} occupying the catalytic metal site is C3'-endo (phase angle of pseudorotation, $P = 29°$). The resultant sugar conformation positions O3' in a near perfect geometry for an in-line attack on the αP of the incoming nucleoside triphosphate. This new position not only completes the octahedral inner coordination sphere for the catalytic Mg^{2+} (Figure 6A), but also situates O3' of the primer terminus within 3.4 Å of the αP of the incoming dCTP (Figure 7). The nucleotide binding Mg^{2+} in site B coordinates nonbridging oxygens from each phosphate (α,β,γ–tridentate) and exhibits good octahedral geometry when site A is occupied by either Na^{+} or Mg^{2+} (Figures 4B and 6B).

Polymerase Metal Coordinating Ligands

Three acidic residues of the catalytic subdomain coordinate the two metals in the ternary substrate complex: Asp190, Asp192, and Asp256 (Figures 6 and 7). Asp190 and Asp192 coordinate both metals and are structurally conserved among members of different polymerase families. In contrast, Asp256 only coordinates metal A, and the equivalent residue in A– and Y–family polymerases is glutamate. Structural alignment of substrate complexes from members of these families, based on the triphosphate moiety of the incoming nucleotide, indicates that these glutamate residues could coordinate a catalytic Mg^{2+} in an alternate conformation. The proposed role of Asp256, or its acidic counterpart in other polymerases, as a general base is controversial (Pelletier, 1994, Steitz et al., 1994). The geometry and position of the catalytic metal provides compelling evidence that it can alter the pK_a of both the primer terminal 3'–OH and Asp256 (Pelletier, 1994). Alanine-substitution for Asp256 abolishes pol β activity demonstrating a critical role of this residue during catalysis (Sobol et al., 2000). Likewise, alanine-substitution for Glu883 in Klenow fragment of *E. coli* DNA polymerase I dramatically decreases the rate of chemistry indicating an important role of this residue in A-family DNA polymerases (Polesky et al., 1992). Since the nature of the metal at site A has a significant influence on the geometry and position of the surrounding oxygen ligands, the identity of the metal occupying the catalytic site is crucial to a structural interpretation of the role of this acidic side chain. In this regard, we note that the average coordinate distance of the ligands for the metal modeled in site A in other reported DNA polymerase structures is greater than 2.35 Å and the coordination number less than that expected for magnesium (n=6) (Table 1). It remains to be determined whether these differences represent alternate cations bound to these sites or if it represent intrinsic differences that may have functional implications.

In the absence of the incoming nucleotide (pol βDNA binary complex), neither metal site is occupied and Asp190, Asp192, and Asp256 are observed in alternate conformations, hydrogen bonding to the primer terminal O3', Arg258, and Arg254, respectively (Sawaya et al., 1997). Additionally, the binding of the correct nucleotide, with its associated Mg^{2+} (metal B), induces subdomain motions and DNA conformational changes that 'close' the nascent base pair pocket necessary for efficient DNA synthesis (Beard and Wilson, 2003). Thus, dNTP/metal B and metal A binding result in crucial conformational changes in the active site. Even subtle alterations in the active site by exchanging the cation in metal site A demonstrates that the polymerase active site is exquisitely sensitive to alternate cations at this site. For example, the conformation of Asp190 and Asp256 and the position of O3′ of the primer terminus are dependent on the identity of the metal occupying this site. Yet, other residues in the vicinity of the incoming nucleotide (e.g., Arg183) are not sensitive to the identity of the metal in site A (Figure 7). Using an exchange inert Cr^{3+}—dNTP complex, a ternary substrate complex structure of pol β was determined where the catalytic metal site is deliberately left empty so

as to trap a the complex where the primer terminus had a 2′-deoxyribose sugar, Table 1 (Arndt et al., 2001). In this situation, Asp256 displays yet another conformation pointing away from the empty catalytic metal binding site.

Concluding Remarks

Based on a two metal mechanism proposed for the 3′–5′ exonuclease activity of the Klenow fragment of *E. coli* DNA polymerase I, Beese and Steitz (Beese and Steitz, 1991) suggested that polymerases might utilize a similar mechanism. Subsequently, the first ternary substrate complex of a DNA polymerase was solved by employing a dideoxy-terminated primer that captured a ternary pol β/DNA/ddCTP complex (Pelletier et al., 1994). Many aspects of this structure support a two-metal mechanism; particularly the observation that active site acidic groups coordinate two divalent metal which are approximately positioned to participate in chemistry. Although magnesium was modeled into the catalytic metal site in that early structure, it was noted that the electron density could have been interpreted as a water molecule. Subsequent ternary complex structures have trapped catalytic intermediates by utilizing a dideoxy-terminated primer (Table 1). In many of these cases, a magnesium ion was modeled into the catalytic metal site even though the number of coordinating ligands and distances were not appropriate for magnesium (Harding, 2001). The lack of a potential coordinating ligand (O3′) would be expected to reduce the affinity and specificity of metal site A, but not site B. In this regard, substrate structures of pol β indicate that Mg^{2+} occupies site B in the presence of an incoming nucleotide regardless whether the incoming nucleotide is ddCTP or dUMPNPP (Figures 1B, 2 and 4B). Likewise, ternary complex structures of pol β determined in the presence of high sodium concentrations indicate that the catalytic metal site is occupied by Na^{+}, rather than Mg^{2+}, independent of the identity of the incoming nucleotide (ddCTP and dUMPNPP) or whether the primer terminus has a 3′-OH (Figures 1B, 2, and 4B). Since the intracellular concentration of sodium is low, this observation is probably not physiologically relevant. However, the results indicate that when ions other than magnesium are bound to the catalytic metal site, the coordination and active site geometry (O3′–Pα distance) are distorted (Figure 7). We have not tried to increase the Mg^{2+} concentration with the ddCTP closed complex to see whether Mg^{2+} can replace Na^{+} in the catalytic metal site.

Nucleophilic substitution reactions at phosphorous are portrayed relative to bond formation/breaking character at the transition state and are expressed in terms of intermediates between associative and dissociative mechanisms. A minimum estimate of the fractional associativity of a mechanism can be calculated from the distance between the attacking atom (3′-O^{-}) and the phosphorous undergoing substitution (Pα) from a ground-state crystal structure (Mildvan, 1997). Assuming a symmetrical trigonal-bipyramidal transition state where the atoms occupying the apical positions (O3′ and $NH^{\alpha-\beta}$) are stationary, the distance between O3′ and Pα would be 2.5 Å, indicating a lower limit of 5.2% associativety for this mechanism.

Kinetic analyses of DNA polymerases from various polymerase families suggest that under some conditions non-chemical steps precede nucleotidyl transfer and limit correct nucleotide insertion (Joyce and Benkovic, 2004). The identity of this step(s) in terms of structural events is unknown. Although there is no definitive evidence indicating that a non-chemical step limits correct nucleotide insertion for pol β, structural (Sawaya et al., 1997) and kinetic studies (Beard et al., 2004) clearly demonstrate that conformational changes occur upon binding substrates for pol β. These events include subdomain motions (Sawaya et al., 1997), sequential protein side-chain rearrangements (Yang et al., 2002), and DNA conformational changes that include template reorientation (Beard and Wilson, 1998). The thermodynamic contribution of these observed conformational changes to the overall fidelity of DNA synthesis remains to be established. A simple change in the sugar pucker of the primer terminus to C3′-endo is sufficient to position O3′ near Pα (Figure 7). Although alterations in sugar pucker are generally very

rapid in solution, it remains to be determined what parameters in the confines of the polymerase active site influence the observed sugar conformation. We demonstrate here that the identity of the ion in site A influences the primer terminus sugar pucker: C3′-endo ($P = 29°$) in the presence of Mg^{2+} and $P \gg 29°$ when Na^{+} occupies this site. The resolution of the Na^{+} complex with dUMPNPP (2.2 Å) precludes unambiguous description of the sugar pucker of the primer terminus. However, the positions of O3′ is clear and indicates that the conformation should be nearer C2′-endo (Figures 4A, 5, and 7). Thus, in addition to the multitude of conformational transitions described previously (Beard and Wilson, 1998, Beard and Wilson, 2003, Pelletier et al., 1994, Sawaya et al., 1997), catalytic magnesium binding induces additional conformational adjustments that bring about proper geometrical alignment necessary for efficient nucleotidyl transfer.

The use of substrate analogs to trap catalytic intermediates for structure determination has been a useful and productive approach. The use of a DNA analog lacking a primer 3′-OH has been used successfully many times (Table 1) since its first application with pol β (Pelletier et al., 1994). We now demonstrate the utility of using a non-hydrolyzable dNTP analog. This approach captures a catalytic intermediate without removing any of the atoms that participate directly during catalysis (primer-O3′, Pα, and Mg^{2+}). Instead, the bridging oxygen between Pα and Pβ is substituted with nitrogen. The nitrogen substitution alters the PA–X3A bond distance and PA–X–PB angle less than 7 and 3% respectively, thereby preserving active site geometry.

The structures reported here reveal the dynamic nature of the polymerase active site (Bose-Basu et al., 2004) as well as the strong influence of the catalytic metal on active site geometry (Yang et al., 2004). The aberrant conformations of mismatched base pairs at the primer terminus (Batra et al., 2005) or nascent base pair binding pocket (Krahn et al., 2004) suggest that misinsertion is deterred by distorting the catalytic metal binding site. The structure of the complete catalytic complex with Mg^{2+} occupying both metal binding sites represents the closest structure to the transition state for a DNA polymerase to date. It is now possible to infer active site adjustments when unnatural metals that reduce fidelity, such as Co^{2+} and Mn^{2+} (Sirover and Loeb, 1976), occupy the metal binding sites. For the first time, we can now begin to confidently examine the precise sequence of events (deprotonation/protonation and bond making/breaking) and the free energy surface of the chemical reaction by computational methods. Finally, the use of dNTP analogs to trap pre-catalytic complexes with other DNA polymerases should uncover general and specific strategies that are utilized to achieve efficient and faithful replication of DNA.

Experimental Procedures

Crystallization of the Pol β Ternary Substrate Complex

Human pol β was over-expressed in *E. coli* and purified (Beard and Wilson, 1995). The DNA substrate consisted of a 16-mer template, a complementary 9- or 10-mer primer strand, and a 5-mer downstream oligonucleotide. The annealed 9-mer primer creates a two-nucleotide gap with two templating G residues. Proper annealing with the 10-mer produces a one-nucleotide gapped DNA substrate with an adenine serving as the templating base. The sequence of the downstream oligonucleotide was 5′–GTCGG–3′ with a phosphorylated 5′-terminus. The template sequence was 5′–CCGAC(A or G)GCGCATCAGC–3′ and the primer sequence was 5′–GCTGATGCG(±C)–3′. Oligonucleotides were dissolved in 20 mM $MgCl_2$, 100 mM Tris/HCl, pH 7.5. Each set of template, primer, and downstream-oligonucleotides was mixed in a 1:1:1 ratio and annealed using a PCR thermocycler by heating 10 min at 90 °C and cooling to 4 °C (1 °C min^{-1}) resulting in a 1 mM mixture of gapped duplex DNA. This solution was then mixed with an equal volume of pol β at 4 °C, the mixture warmed to 35 °C and gradually cooled

to 4 °C. A four-fold molar excess of ddCTP was added to the 2-nucleotide gapped DNA to produce the ternary DNA/ddCTP complex.

Pol β-DNA complexes were crystallized by sitting drop vapor diffusion. The reservoir solution for formation of the ternary DNA/ddCTP complex consisted of 50 mM HEPES, pH 7.5, 180 mM sodium acetate and 16% PEG-3350. The crystallization buffers for binary one-nucleotide gapped DNA complexes were 16% PEG-3350, 350 mM sodium acetate, and 50 mM imidazole, pH 7 or 100 mM imidazole, pH 8. Drops were incubated at 18 °C and streak seeded after 1 day. Crystals grew in approximately 2 to 4 days after seeding. The crystals of the ternary DNA/ddCTP complex were transferred to cryo-protectant solutions containing 50 mM HEPES, pH 7.5, 180 mM sodium acetate, 12% ethylene glycol and 20% PEG-3350. The crystals of the binary one-nucleotide gapped DNA complex were soaked in artificial mother liquor with10 mM $MgCl_2$, 1 mM dUMPNPP (Jena Bioscience), 20% PEG-3350, and 12% ethylene glycol. To saturate Mg^{2+} binding to the catalytic site, the $[Mg^{2+}]/[Na^{+}]$ in the soaking solution was increased by lowering the sodium acetate concentration to 90 mM, and increasing $MgCl_2$ to 200 mM. All three crystals belong to the space group $P2_1$.

Data Collection and Structure Determination

Data were collected at 100 K on an R-Axis IV area detector system mounted on a RUH3R rotating anode generator or at the Advanced Photon Source (APS, SER-CAT 22-ID). Data were integrated and reduced with HKL2000 software (Otwinowski and Minor, 1997).

Ternary substrate complex structures were determined by molecular replacement with a previously determined structure of pol β complexed with one-nucleotide gapped DNA and a complementary incoming ddCTP, PDB accession 1BPY (Sawaya et al., 1997). The crystal structures have similar lattices and are sufficiently isomorphous to determine the molecular-replacement model position by rigid body refinement. The parameters and topology for dUMPNPP were based on CNS libraries with parameters for the P–N–P fragments derived from analysis of several well-characterized small molecule structures (Cambridge Structure Database). Nucleic acid backbone and sugar pucker dihedral restraints were excluded in later stages of refinement because CNS enforces standardized A/B-form geometries, whereas several residues in these structures exhibit alternate geometries (Krahn et al., 2004). Refinement statistics are given in Table 2. The figures were prepared in Chimera (Pettersen et al., 2004) or Molscript/Raster3D (Kraulis, 1991, Merritt and Bacon, 1997).

Kinetic Assays

DNA synthesis was assayed on a single-nucleotide gapped DNA substrate where the templating base in the gap was an adenine. The DNA sequence was as described previously (Beard et al., 2004) with the core sequence identical to that used for crystallization. Enzyme activities were determined using a reaction mixture containing 50 mM Tris-HCl, pH 7.4, 20 mM $MgCl_2$, 200 nM single-nucleotide gapped DNA, and various dUTP or dTTP concentrations. Reactions were initiated with 0.5 nM enzyme at room temperature and stopped with EDTA mixed with formamide dye. The substrates and products were separated on 15% denaturing polyacrylamide gels and quantified in the dried gels by phosphorimagery. Steady-state kinetic parameters were determined by fitting the rate data to the Michaelis equation. Inhibition of dTTP insertion by dUMPNPP was determined at various concentrations of inhibitor and sub-saturating dTTP concentrations.

Acknowledgements

We thank Zhongmin Jin for assistance in data collection at Southeast Regional Collaborative Access Team (SER-CAT) 22-ID beamline at the Advanced Photon Source, Argonne National Laboratory. Use of the Advanced Photon Source was supported by the U. S. Department of Energy, Office of Science, Office of Basic Energy Sciences, under Contract No. W-31-109-Eng-38. This research was supported by the Intramural Research Program of the NIH, National

Institute of Environmental Health Sciences and the National Institutes of Health Grant 1U19CA105010. We also thank L.G. Pedersen and P. Lin for critical reading of the manuscript.

References

Arndt JW, Gong W, Zhong X, Showalter AK, Liu J, Dunlap CA, Lin Z, Paxson C, Tsai MD, Chan MK. Insight into the catalytic mechanism of DNA polymerase β: Structures of intermediate complexes. Biochemistry 2001;40:5368–5375. [PubMed: 11330999]

Batra VK, Beard WA, Shock DD, Pedersen LC, Wilson SH. Nucleotide-induced DNA polymerase active site motions accomodating a mutagenic DNA intermediate. Structure (Camb) 2005;13:1225–1233. [PubMed: 16084394]

Beard WA, Wilson SH. Purification and domain-mapping of mammalian DNA polymerase β. Methods Enzymol 1995;262:98–107. [PubMed: 8594388]

Beard WA, Wilson SH. Structural insights into DNA polymerase β fidelity: Hold tight if you want it right. Chem Biol 1998;5:R7–R13. [PubMed: 9479474]

Beard WA, Wilson SH. Structural design of a eukaryotic DNA repair polymerase: DNA polymerase β. Mutat Res 2000;460:231–244. [PubMed: 10946231]

Beard WA, Shock DD, Vande Berg BJ, Wilson SH. Efficiency of correct nucleotide insertion governs DNA polymerase fidelity. J Biol Chem 2002;277:47393–47398. [PubMed: 12370169]

Beard WA, Wilson SH. Structural insights into the origins of DNA polymerase fidelity. Structure (Camb) 2003;11:489–496. [PubMed: 12737815]

Beard WA, Shock DD, Wilson SH. Influence of DNA structure on DNA polymerase β active site function: Extension of mutagenic DNA intermediates. J Biol Chem 2004;279:31921–31929. [PubMed: 15145936]

Beese LS, Steitz TA. Structural basis for the 3′–5′ exonuclease activity of *Escherichia coli* DNA polymerase I: a two metal ion mechanism. EMBO J 1991;10:25–33. [PubMed: 1989886]

Bose-Basu B, DeRose EF, Kirby TW, Mueller GA, Beard WA, Wilson SH, London RE. Dynamic characterization of a DNA repair enzyme: NMR studies of [*methyl*-^{13}C]methionine-labeled DNA polymerase β. Biochemistry 2004;43:8911–8922. [PubMed: 15248749]

Brieba LG, Eichman BF, Kokoska RJ, Doublie S, Kunkel TA, Ellenberger T. Structural basis for the dual coding potential of 8-oxoguanosine by a high-fidelity DNA polymerase. EMBO J 2004;23:3452–3461. [PubMed: 15297882]

Doublié S, Tabor S, Long AM, Richardson CC, Ellenberger T. Crystal structure of a bacteriophage T7 DNA replication complex at 2.2 Å resolution. Nature 1998;391:251–258. [PubMed: 9440688]

Franklin MC, Wang J, Steitz TA. Structure of the replicating complex of a pol α family DNA polymerase. Cell 2001;105:657–667. [PubMed: 11389835]

Garcia-Diaz M, Bebenek K, Krahn JM, Kunkel TA, Pedersen LC. A closed conformation for the Pol λcatalytic cycle. Nature Struct Mol Biol 2005;12:97–98. [PubMed: 15608652]

Harding MM. Geometry of metal-ligand interactions in proteins. Acta Crystallographica Section D 2001;57:401–411.

Harding MM. Metal-ligand geometry relevant to proteins and in proteins: sodium and potassium. Acta Crystallographica D 2002;58:872–874.

Huang H, Chopra R, Verdine GL, Harrison SC. Structure of a covalently trapped catalytic complex of HIV-1 reverse transcriptase: Implications for drug resistance. Science 1998;282:1669–1675. [PubMed: 9831551]

Johnson SJ, Taylor JS, Beese LS. Processive DNA synthesis observed in a polymerase crystal suggests a mechanism for the prevention of frameshift mutations. Proc Natl Acad Sci USA 2003;100:3895–3900. [PubMed: 12649320]

Joyce CM, Benkovic SJ. DNA polymerase fidelity: Kinetics, structure, and checkpoints. Biochemistry 2004;43:14317–14324. [PubMed: 15533035]

Krahn JM, Beard WA, Miller H, Grollman AP, Wilson SH. Structure of DNA polymerase β with the mutagenic DNA lesion 8-oxodeoxyguanine reveals structural insights into its coding potential. Structure (Camb) 2003;11:121–127. [PubMed: 12517346]

Krahn JM, Beard WA, Wilson SH. Structural insights into DNA polymerase deterrents for misincorportion support an induced-fit mechanism for fidelity. Structure (Camb) 2004:1823–1832. [PubMed: 15458631]

Kraulis P. MOLSCRIPT: a program to produce both detailed and schematic plots of proteins. J Appl Cryst 1991;24:946–950.

Li Y, Korolev S, Waksman G. Crystal structures of open and closed forms of binary and ternary complexes of the large fragment of *Thermus aquaticus* DNA polymerase I: structural basis for nucleotide incorporation. EMBO J 1998;17:7514–7525. [PubMed: 9857206]

Li Y, Mitaxov V, Waksman G. Structure-based design of *Taq* DNA polymerases with improved properties of dideoxynucleotide incorporation. Proc Natl Acad Sci USA 1999;96:9491–9496. [PubMed: 10449720]

Li Y, Dutta S, Doublié S, Bdour HMd, Taylor JS, Ellenberger T. Nucleotide insertion opposite a *cis-syn* thymine dimer by a replicative DNA polymerase from bacteriophage T7.1 2004;1:784–790.

Ling H, Boudsocq F, Woodgate R, Yang W. Crystal structure of a Y-family DNA polymerase in action: A mechanism for error-prone and lesion-bypass replication. Cell 2001;107:91–102. [PubMed: 11595188]

Lovell SC, Davis IW, Arendall WB III, de Bakker PIW, Word JM, Prisant MG, Richardson JS, Richardson DC. Structure validation by Cα geometry:φ, psi; and Cβ deviation. Proteins 2003;50:437–450. [PubMed: 12557186]

Merritt EA, Bacon DJ. Raster3D: Photorealistic molecular graphics. Methods Enzymol 1997;277:505–524.

Mildvan AS. Mechanisms of signaling and related enzymes. Proteins 1997;29:401–416. [PubMed: 9408938]

Müller P, Kopke S, Sheldrick GM. Is the bond-valence method able to identify metal atoms in protein structures? Acta Crystallographica D 2003;59:32–37.

Nair DT, Johnson RE, Prakash L, Prakash S, Aggarwal AK. Rev1 employs a novel mechanism of DNA synthesis using a protein template. Science 2005a;309:2219–2222. [PubMed: 16195463]

Nair DT, Johnson RE, Prakash L, Prakash S, Aggarwal AK. Human DNA polymerase τ incorporates dCTP opposite template G via a G.C+ Hoogsteen base pair. Structure (Camb) 2005b;13:1569–1577. [PubMed: 16216587]

Otwinowski Z, Minor W. Processsing of X-ray diffraction data collected in oscillation mode. Methods Enzymol 1997;276:307–326.

Pelletier H. Polymerase structures and mechanism. Science 1994;266:2025–2026. [PubMed: 7801132]

Pelletier H, Sawaya MR, Kumar A, Wilson SH, Kraut J. Structures of ternary complexes of rat DNA polymerase β, a DNA template-primer, and ddCTP. Science 1994;264:1891– 1903. [PubMed: 7516580]

Pettersen EF, Goddard TD, Huang CC, Couch GS, Greenblatt DM, Meng EC, Ferrin TE. UCSF Chimera—A visualization system for exploratory research and analysis. J Comput Chem 2004;25:1605–1612. [PubMed: 15264254]

Polesky AH, Dahlberg ME, Benkovic SJ, Grindley ND, Joyce CM. Side chains involved in catalysis of the polymerase reaction of DNA polymerase I from *Escherichia coli*. J Biol Chem 1992;267:8417–8428. [PubMed: 1569092]

Prasad R, Batra VK, Yang X-P, Krahn JM, Pedersen LC, Beard WA, Wilson SH. Structural insightr into the DNA polymertase β deoxyribose phosphate lyase mechanism. DNA Repair. 2005in press

Sawaya MR, Pelletier H, Kumar A, Wilson SH, Kraut J. Crystal structure of rat DNA polymerase β: Evidence for a common polymerase mechanism. Science 1994;264:1930– 1935. [PubMed: 7516581]

Sawaya MR, Prasad P, Wilson SH, Kraut J, Pelletier H. Crystal structures of human DNA polymerase β complexed with gapped and nicked DNA: Evidence for an induced fit mechanism. Biochemistry 1997;36:11205–11215. [PubMed: 9287163]

Sirover MA, Loeb LA. Infidelity of DNA synthesis in vitro: Screening for potential metal mutagens or carcinogens. Science 1976;194:1434–1436. [PubMed: 1006310]

Sobol RW, Prasad R, Evenski A, Baker A, Yang XP, Horton JK, Wilson SH. The lyase activity of the DNA repair protein β-polymerase protects from DNA-damage-induced cytotoxicity. Nature 2000;405:807–810. [PubMed: 10866204]

Steitz TA, Smerdon S, Jäger J, Wang J, Kohlstaedt LA, Friedman JM, Beese LS, Rice PA. Two DNA polymerases: HIV reverse transcriptase and the Klenow fragment of *Escherichia coli* DNA polymerase I. Cold Spring Harb. Symp Quant Biol 1993;58:495–504.

Steitz TA, Smerdon SJ, Jager J, Joyce CM. A unified polymerase mechanism for nonhomologous DNA and RNA polymerases. Science 1994;266:2022–2025. [PubMed: 7528445]

Steitz TA. DNA polymerases: Structural diversity and common mechanisms. J Biol Chem 1999;274:17395–17398. [PubMed: 10364165]

Wang J. DNA polymerases: Hoogsteen base-pairing in DNA replication? Nature 2005;437:E6–E7. [PubMed: 16163299]

Yang L, Beard WA, Wilson SH, Broyde S, Schlick T. Polymerase β simulations suggest that Arg258 rotation is a slow step rather than large subdomain motions *per se*. J Mol Biol 2002;317:679–699.

Yang L, Arora K, Beard WA, Wilson SH, Schlick T. Critical Role of magnesium ions in DNA polymerase β's closing and active site assembly. J Am Chem Soc 2004;126:8441–8453. [PubMed: 15238001]

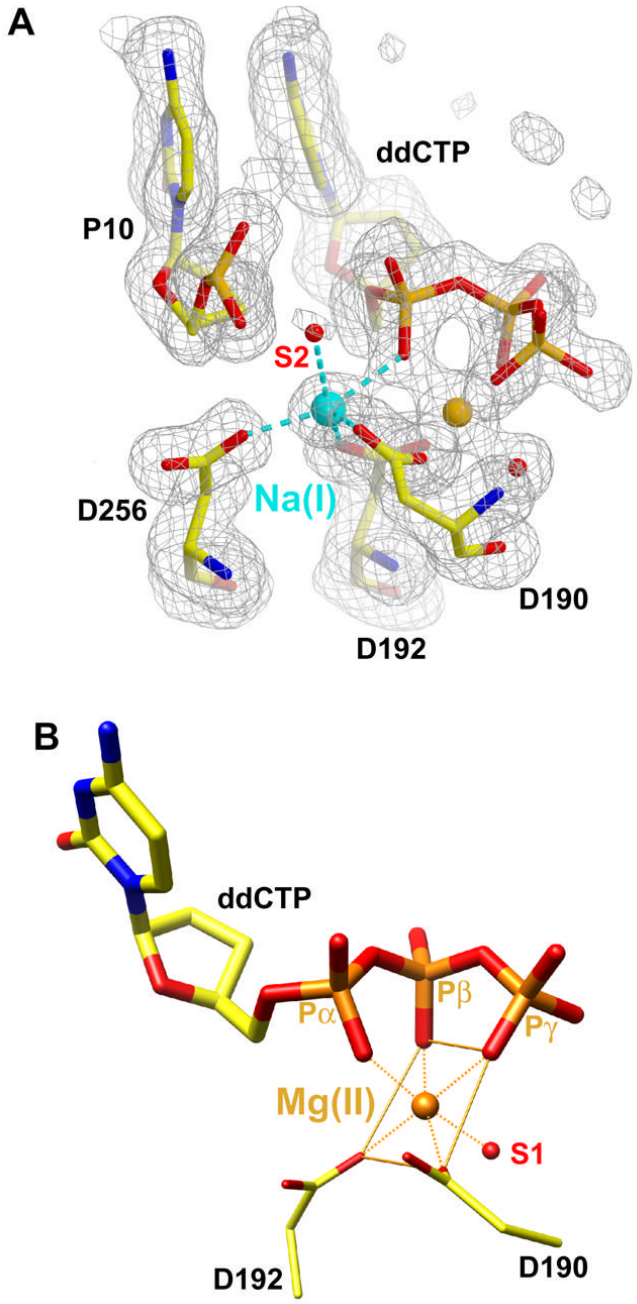

Figure 1. Active Site Coordination of the Ions Observed in a High-Resolution (1.65 Å) DNA Polymerase β /DNA/ddCTP Teranry Complex

(A) A F_o-F_c simulated annealing electron density omit map (gray) contoured at 2.5σ for the pol β active site. A penta-coordinated ion is bound to the catalytic metal site. The coordination distances (Table 3) are consistent with the identity of this ion as Na^+ (light blue). Additionally, a previously postulated water molecule (S2) is now observed. The Na^+ is also coordinated by all three active site aspartates (D190, D192, D256) and a non-bridging oxygen on Pα (pro-R_P oxygen). The nucleotide binding metal is consistent with Mg^{2+} (orange). The density is superimposed on the refined modeled primer terminus (P10), incoming nucleotide (ddCTP), active site aspartates (D190, D192, D256), and a nucleotide metal-coordinating water. The

primer terminus O3' is believed to be the sixth ligand, but was omitted to trap the catalytic intermediate for structure determination.

(B) The octahedral coordination and coordination distances (Table 3) of the ion in the nucleotide binding metal site is consistent with the identity of this ion as Mg^{2+}. The metal is coordinated to non-bridging oxygens on all three phosphates of the incoming ddCTP (α,β ,γ-tridentate). In addition, Asp190 (D190), Asp192 (D192), and a water molecule (S1) completes the inner coordination sphere.

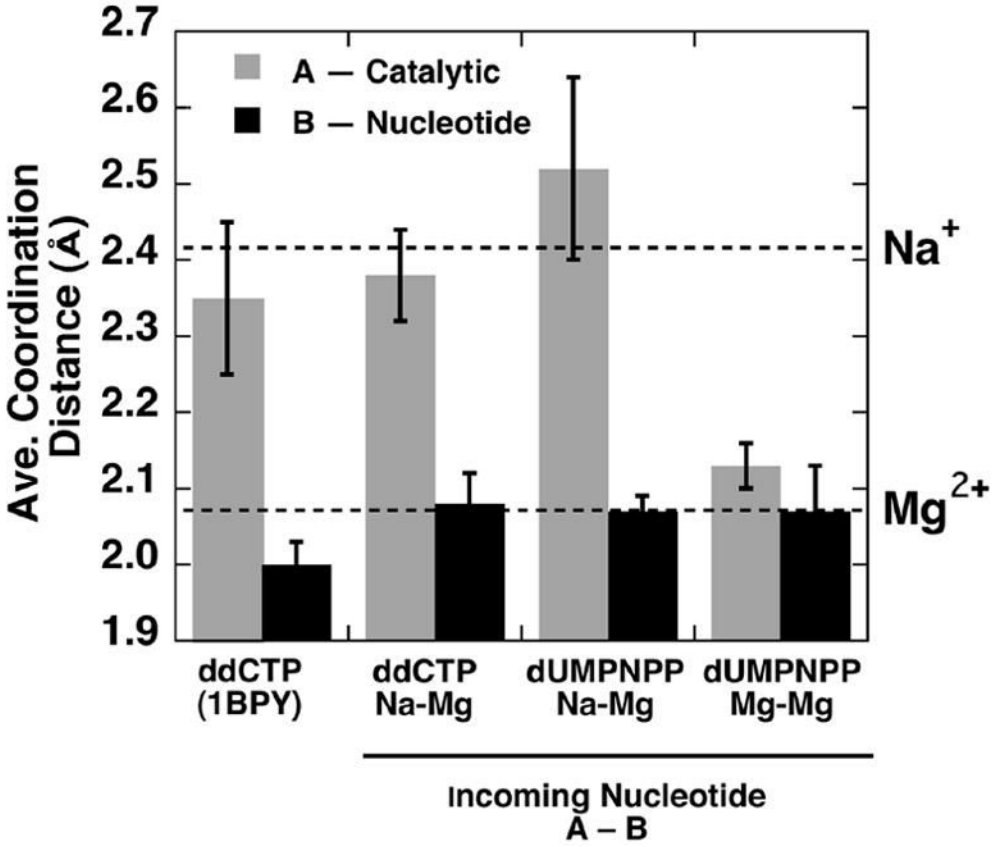

Figure 2.

Average Coordination Distances for the Oxygen Ligands to the Catalytic (A) or Nucleotide Binding (B) Metals

These distances are computed for a previously reported structure of pol β (1BPY) (Sawaya et al., 1997), the 1.65 Å structure (ddCTP/Na–Mg; 2FMP), and two ternary substrate complex structures trapped with the dUMPNPP non-hydrolyzable analogue (Na–Mg, 2FMQ; Mg–Mg, 2FMS). The substrate complex structures are denoted by the identity of the incoming nucleotide and the putative ions in sites A and B. The specific coordinating atoms and distances are tabulated in Table 3. The errors bars represent the standard errors of the calculated averages. The horizontal dashed lines indicate the coordinate distances observed from accurately determined small molecule structures (Harding, 2001, Harding, 2002).

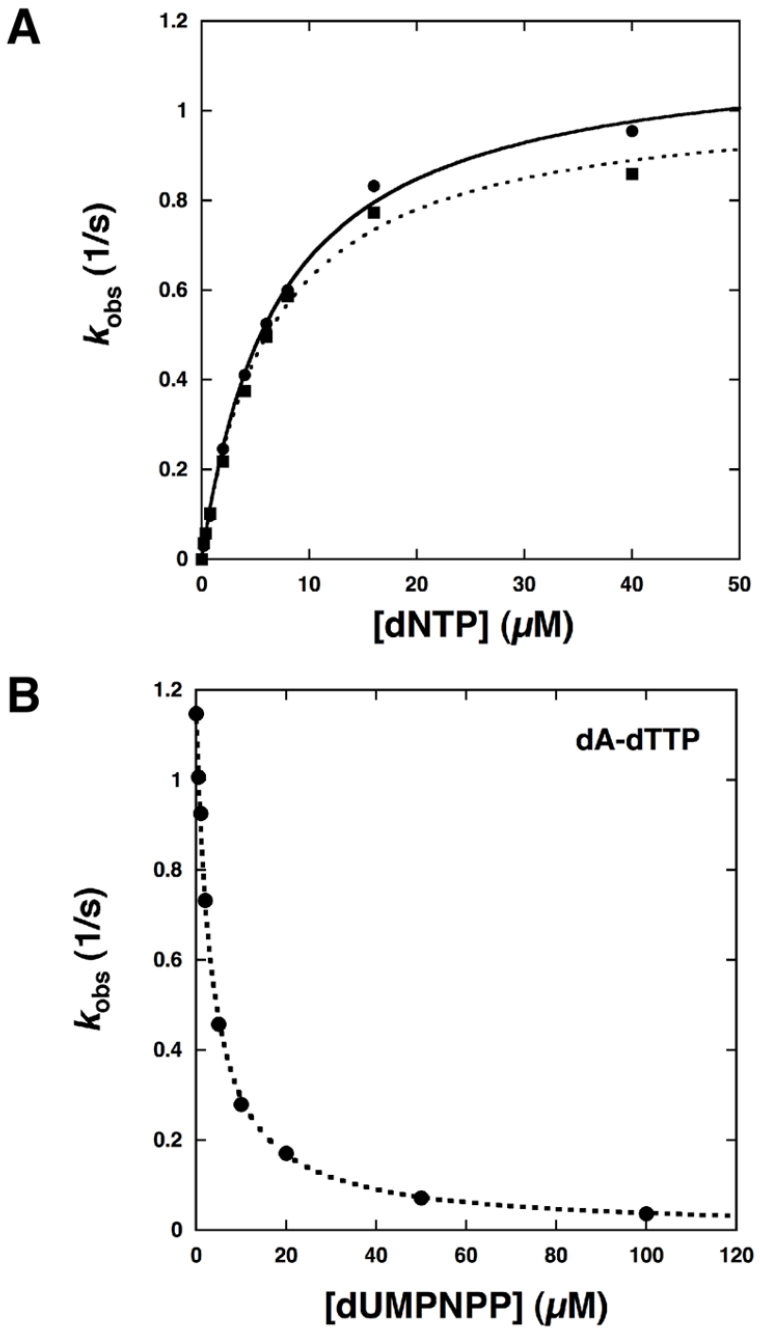

Figure 3. Kinetic Analysis of dUTP Insertion and dUMPNPP Inhibiiton

(A) Steady-state kinetic analysis indicates that dUTP insertion (■) is similar to that for dTTP (●). The catalytic efficiencies (k_{cat}/K_m) for dTTP and dUTP insertion are 0.19 ± 0.03 and 0.15 ± 0.02 1/μM–s, respectively, for at least two independent determinations.

(B) Dixon analysis for competitive inhibition indicates that the K_i for dUMPNPP is 0.9 μM (dotted line).

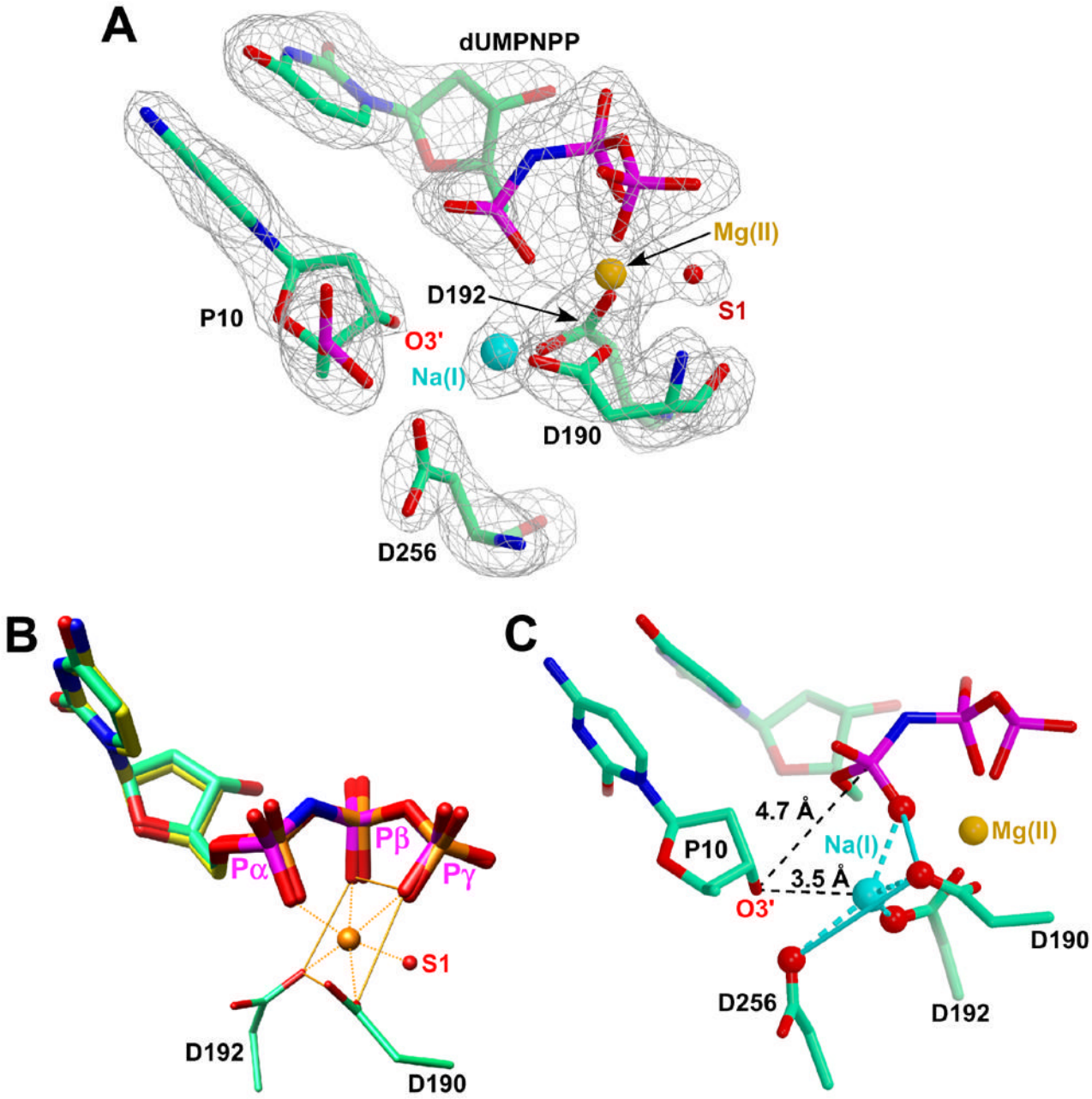

Figure 4. Active Site Geometry of the Ternary DNA Polymerase β /DNA/dUMPNPP Complex with Na^+ in the Catalytic Metal Site

(A) The F_o-F_c simulated annealing electron density omit map (gray) contoured at 3.8σ for the pol β active site with Na^+ (light blue) occupying the catalytic site. The nucleotide binding metal is consistent with Mg^{2+} (orange). The density is superimposed on the refined modeled primer terminus (P10), incoming nucleotide analogue (dUMPNPP), active site aspartates (D190, D192, D256), and the nucleotide metal-coordinating water (S1). The density for O3' is clearly observed but distant from the sodium ion in the catalytic metal site.

(B) The ternary substrate complex structures of pol β with an incoming ddCTP (yellow carbon and orange phosphates atoms) and dUMPNPP (green carbon and magenta phosphate atoms) were superimposed with the catalytic subdomains (RMSD = 0.13 Å for 344 atom pairs). The

superimposed structures clearly indicate that the bridging nitrogen (blue) between Pα and Pβ does not significantly alter the position of the phosphates. The octahedral coordination and coordination distances (Table 3) of the ion in the nucleotide binding metal site is consistent with the identity of this ion as Mg^{2+}.

(C) The Na^{+} (light blue) occupying the catalytic metal site displays a distorted coordination geometry. The four coordinating oxygens are displayed as red balls. The primer terminus (P10) O3' is too distant (3.5 Å) for Na^{+} to participate in its coordination. Furthermore, O3' is 4.7 Å from Pα of the incoming nucleotide analog.

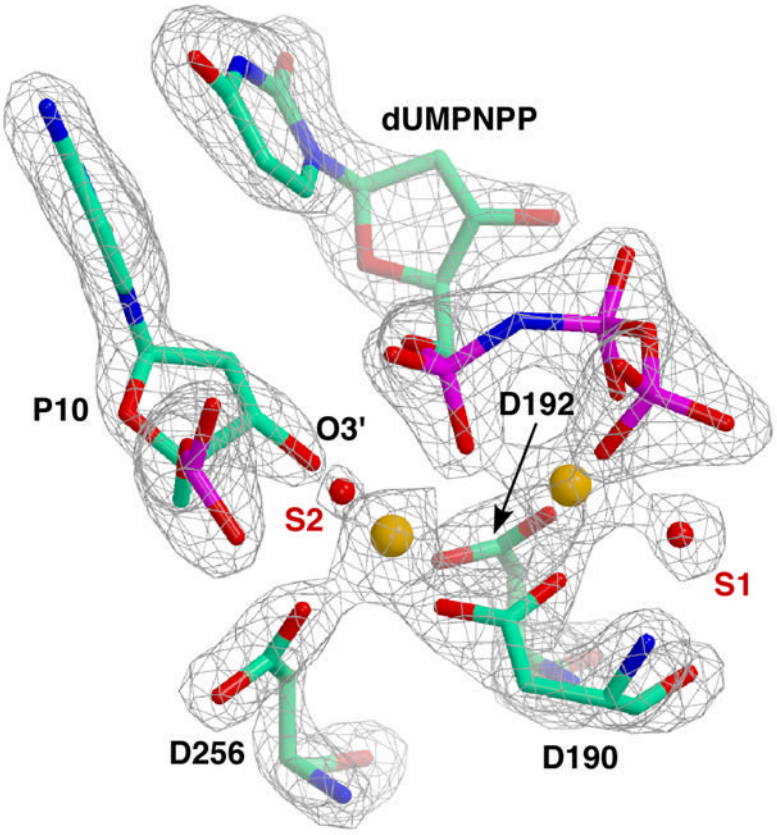

Figure 5. Active Site Geometry of the Ternary DNA Polymerase β /DNA/dUMPNPP Complex with Mg^{2+} in the Catalytic Metal Site

The F_o-F_c simulated annealing electron density omit map (gray) contoured at 4.7σ for the pol β active site with Mg^{2+} (orange) occupying both the catalytic and nucleotide metal binding sites. The density is superimposed on the refined modeled primer terminus (P10), incoming nucleotide analogue (dUMPNPP), active site aspartates (D190, D192, D256), and the metal-coordinating waters (S1 and S2). The density for O3' is clearly observed and the resulting C3'-endo sugar pucker positions O3' near the catalytic metal and Pα of dUMPNPP.

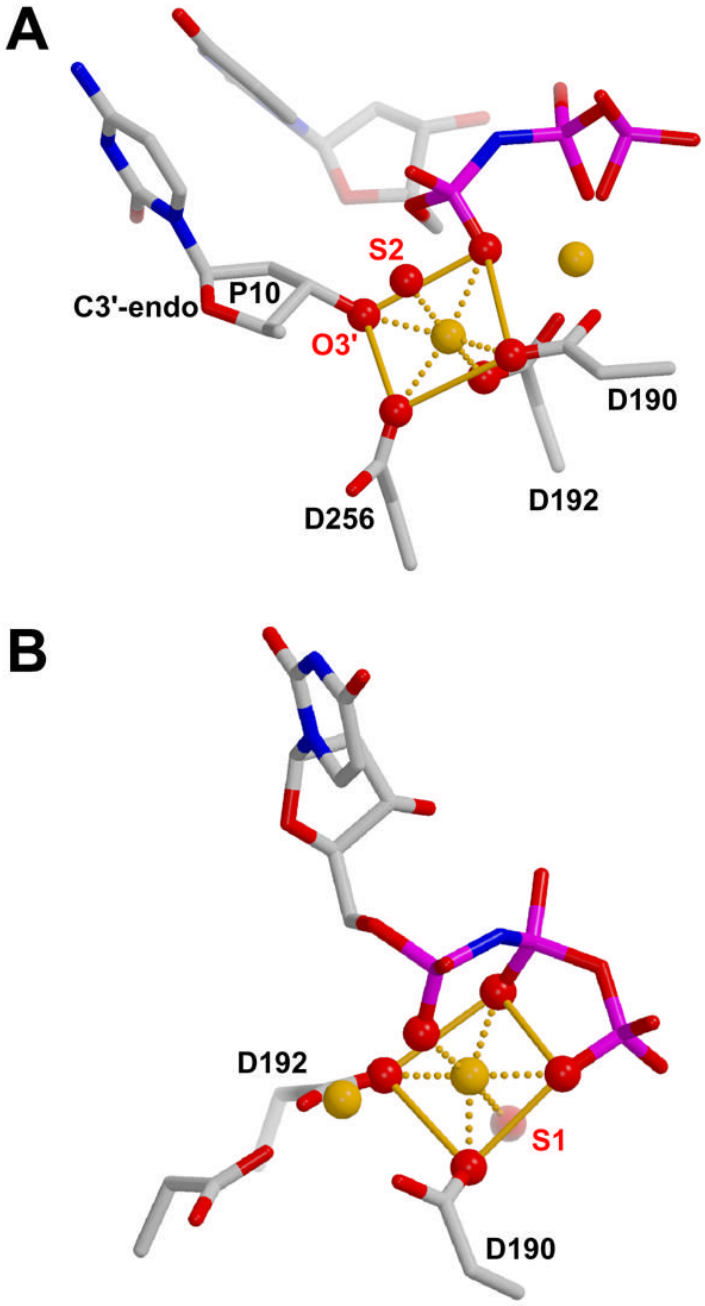

Figure 6. Coordination Geometry of the Metal Binding Sites in the Complete Pre-Catalytic Complex

(A) Coordination geometry of Mg^{2+} (orange) occupying the catalytic metal site. The sugar pucker of the primer terminus (P10) is C3'-endo and the catalytic metal exhibits good octahedral geometry. Additionally, a water molecule (S2) not observed in the lower resolution Na^{+} structure is visible and participates in the first coordination sphere of the catalytic Mg^{2+}. (B) The Mg^{2+} occupying the nucleotide metal site also exhibits good octahedral geometry even when the catalytic site is occupied by Na^{+} (Figure 4B).

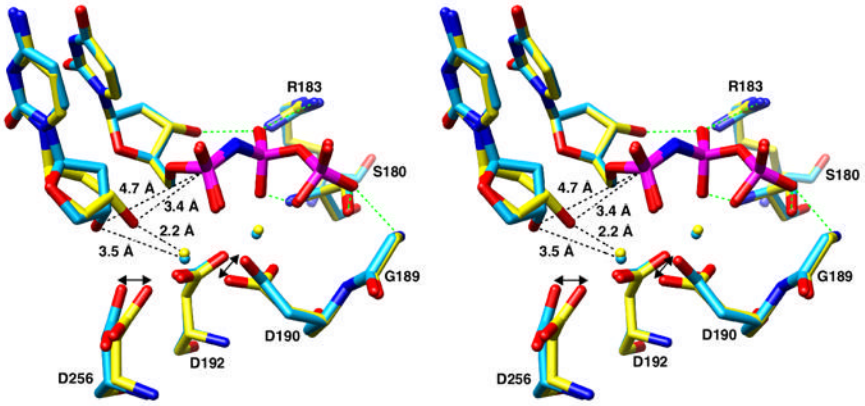

Figure 7. Stereo View of the Pol β Active Site

Superimposed structures of pol β with either Na^+ (light blue) or Mg^{2+} (yellow) in the catalytic metal site A. Residues that hydrogen bond (green) to the triphosphate moiety of the incoming nucleotide and the active site aspartates are shown. When Na^+ occupies the catalytic metal site, O3' of the primer terminus is 3.5 and 4.7 Å from the catalytic metal and αP of the incoming nucleotide, respectively. In contrast, with Mg^{2+} in the catalytic metal site, an altered sugar pucker positions O3' of the primer terminus 2.2 and 3.4 Å from the catalytic metal and Pα of the incoming nucleotide, respectively.

Table 1

Summary of the Metal Active Site Coordination Sphere of DNA Polymerase Undamaged DNA/d(d)NTP Ternary Complex Structures[a]

DNA Polymerase (Family)	NTP	Catalytic (A)			Nucleotide (B)			Resolution	PDB ID (Ref.)
		Me	x[b]	n[c]	Me	x	n		
			Å			Å		Å	
Klentaq (A)	ddCTP	Mg	2.37 (0.07)	5	Mg	2.22 (0.04)	6	2.30	3KTQ (Li et al., 1998)
	ddGTP	Mg	2.46 (0.09)	5	Mg	2.33 (0.06)	6	2.30	1QSS (Li et al., 1999)
	ddATP	Mg	2.48 (0.03)	5	Mg	2.21 (0.05)	6	2.30	1QSY (Li et al., 1999)
	ddTTP	Mg	2.44 (0.05)	5	Mg	2.24 (0.03)	6	2.30	1QTM (Li et al., 1999)
T7 (A)	ddGTP	Mg	2.40 (0.04)	5	Mg	2.27 (0.03)	6	2.20	1T7P (Doublié et al., 1998)
	ddATP	Mg	2.58 (0.06)	5	Mg	2.29 (0.03)	6	2.40	1SKR (Li et al., 2004)
	ddCTP	Mg	2.52 (0.09)	5	Mg	2.34 (0.04)	6	2.54	1T8E (Brieba et al., 2004)
BF (A)	dCTP	Mg	2.75 (0.09)	3	Mn	2.23 (0.12)	6	1.95	1LV5 (Johnson et al., 2003)
RB69 (B)	dTTP	Ca	3.08 (0.09)	4	Ca	2.66 (0.02)	7	2.60	1IG9 (Franklin et al., 2001)
HIV-1 RT (RT)	dTTP	Mg	2.71 (0.21)	3	Mg	2.36 (0.07)	6	3.20	1RTD (Huang et al., 1998)
β (X)	ddCTP	Mg[d]	2.35 (0.01)	4	Mg	2.00 (0.03)	6	2.20	1BPY (Sawaya et al., 1997)
	dTMPPCP	—[e]	—	—	Cr	2.15 (0.05)	5	2.60	1HUO (Arndt et al., 2001)
λ (X)	ddTTP	—	—	—	Mg	2.06 (0.05)	6	1.95	1XSN (Garcia-Diaz et al., 2005)
Dpo4 (Y)	ddGTP	Mg	2.41 (0.20)	4	Ca	2.34 (0.04)	6	2.10	1JXL (Ling et al., 2001)
τ (Y)	dTTP	—	—	—	Mg	2.41 (0.08)	6	2.30	1ZET (Wang, 2005)
τ (Y)	dCTP	Mg	2.66 (0.20)	4	Mg	2.21 (0.04)	6	2.50	1ALZ (Nair et al., 2005b)
REV1 (Y)	dCTP	Mg	2.57 (0.06)	4	Mg	2.28 (0.05)	6	2.30	2AQ4 (Nair et al.,

[a] Except for the Dpo4 and pol β(dTMPPCP) structures, the 3'-primer termini in these structures lack O3' (dideoxy-terminated).

[b] Average coordination distance (SE).

[c] Coordination number (oxygen ligands <3.5 Å). In some instances, both oxygens of the active site aspartates were near metal A or B. In these cases, the closest oxygen was assumed to be the preferred ligand.

[d] The identity of this ion is now believed to be Na^+ (Figure 2).

[e] Metal not observed.

Table 2

Crystallographic Statistics

Complex A–B[a]	**ddCTP Na^+–Mg^{2+}**	**dUMPNPP Na^+–Mg^{2+}**	**dUMPNPP Mg^{2+}–Mg^{2+}**
Data Collection			
a (Å)	50.9	50.8	50.8
b (Å)	80.4	80.2	80.4
c (Å)	55.3	55.3	55.5
β (°)	107.2	107.5	107.9
d_{min}(Å)	1.65 (1.71–1.65)[b]	2.20 (2.28–2.20)	2.00 (2.07–2.00)
R_{merge}(%)[c]	4.1 (24.9)[d]	7.2 (43.2)	6.4 (50.1)
Completeness (%)	97.5 (86.5)	98.8 (97.2)	99.7 (97.9)
I/σ_I	22.8 (4.2)	15.0 (3.8)	10.6 (2.0)
Number of observed reflections	349479	123108	118197
Number of unique reflections	50030	21443	28459
Radiation source	Rigaku RUH3R	Rigaku RUH3R	APS
Wavelength	1.5418	1.5418	0.9997
Refinement			
Rms deviations			
Bond lengths (Å)	0.007	0.005	0.005
Bond angles (°)	1.020	1.050	1.050
R_{work}(%)[e]	18.7	19.0	19.6
R_{free}(%)[f]	21.9	24.3	24.4
Average B factor (Å^2)			
Protein	20.0	30.0	34.1
DNA	24.8	37.0	38.3
Metal A	15.0	29.6	21.5
Metal B	10.6	18.3	17.5
Ramachandran analysis (%)[g]			
Favored	97.8	98.8	98.2
Allowed	100.0	100.0	100.0

[a] Refers to the incoming nucleoside triphosphate of the ternary substrate complex. The metals refer to those identified in the catalytic (A) and nucleotide metal (B) binding sites.

[b] Values in parentheses refer to the highest resolution shell.

[c] $R_{merge} = 100 \times \sum h \sum i |I_{h,i} - I_h| \sum h \sum i I_{h,i}$, where I_h is the mean intensity of symmetry-related reflections $I_{h,i}$.

[d] Numbers in parentheses refer to the highest resolution shell of data (10%).

[e] $R_{work} = 100 \times \sum ||F_{obs}| - |F_{calc}|| / \sum |F_{obs}|$

[f] R_{free} for a 5% subset of reflections withheld from refinement.

[g] As determined by MolProbity (Lovell et al., 2003).

Table 3

Active Site Metal Coordination Distances (Å)

Ternary Complex A–B[a]	ddCTP[b] Na^+–Mg^{2+}	ddCTP Na^+–Mg^{2+}	dUMPNPP Na^+–Mg^{2+}	dUMPNPP Mg^{2+}–Mg^{2+}
Metal A				
P10 (O3')	—[c]	—[c]	3.5	2.2
D190 (OD2)	2.2	2.3	2.6	2.1
D192 (OD1)	2.0	2.2	2.2	2.2
D256 (OD2)	2.6	2.4	2.8	2.1
NTP (O1A)	2.4	2.5	2.5	2.2
H_2OS2(O)	—[d]	2.5	—[d]	2.2
Metal B				
NTP (O1A)	1.9	2.1	2.1	2.1
NTP (O2B)	2.1	2.0	2.0	2.0
NTP (O3G)	2.0	2.1[e]	2.1	2.1
D190 (OD1)	2.0	2.1	2.1	1.9
D192 (OD2)	2.0	2.0	2.0	2.0
H_2OS1 (O)	2.0	2.2	2.1	2.3

[a] Refers to the incoming nucleoside triphosphate of the ternary substrate complex. The metals refer to those identified in the catalytic and nucleotide metal binding sites; metal A and B, respectively.

[b] From Sawaya et al. (Sawaya et al., 1997); pdb accession code 1BPY. Metal A was originally identified as Mg^{2+}, but the coordination distances are more consistent with Na^+ occupying this site.

[c] The sugar at the primer terminus lacks a 3'-OH.

[d] This solvent molecule was not observed.

[e] Pγ exhibited 50% occupancy; accordingly, this distance represents the average distance between O3G and a water molecule at this position.